The Impact of Source Time Function Complexity on Stress-Drop Estimates

James S. Neely*1¹⁰, Sunyoung Park¹⁰, and Annemarie Baltay²

ABSTRACT

Earthquake stress drop—a key parameter for describing the energetics of earthquake rupture—can be estimated in several different, but theoretically equivalent, ways. However, independent estimates for the same earthquakes sometimes differ significantly. We find that earthquake source complexity plays a significant role in why theoretically (for simple rupture models) equivalent methods produce different estimates. We apply time- and frequency-domain methods to estimate stress drops for real earthquakes in the SCARDEC (Seismic source ChAracteristics Retrieved from DEConvolving teleseismic body waves, Vallée and Douet, 2016) source time function (STF) database and analyze how rupture complexity drives stress-drop estimate discrepancies. Specifically, we identify two complexity metrics—Brune relative energy (BRE) and spectral decay—that parameterize an earthquake's complexity relative to the standard Brune model and strongly correlate with the estimate discrepancies. We find that the observed systematic magnitude-stress-drop trends may reflect underlying changes in STF complexity, not necessarily trends in actual stress drop. Both the decay and BRE parameters vary systematically with magnitude, but whether this magnitude-complexity relationship is real remains unresolved.

KEY POINTS

- Theoretically equivalent earthquake stress-drop methods often produce conflicting estimates.
- Source time function complexity can explain discrepancies among different estimates.
- Apparent magnitude–stress-drop trends may reflect systematic variations in earthquake complexity instead.

INTRODUCTION

Earthquake stress drop, the change in stress along a fault before and after an earthquake, is thought to provide an insight into the rupture characteristics of earthquakes (e.g., Abercrombie, 2021), the resulting ground motions that they produce (e.g., Boore, 1983), and is a key parameter in earthquake rupture modeling (e.g., Causse et al., 2014). Systematic differences in stress drop by tectonic environment have been previously observed (e.g., Kanamori and Anderson, 1975; Allmann and Shearer, 2009; Courboulex et al., 2016), as have magnitudedepth-dependent variations (see references Abercrombie, 2021) and variations caused by lithology (e.g., Kemna et al., 2021). However, different studies often find conflicting results even when the same earthquakes, and even the same waveforms, are examined (e.g., Neely et al., 2020).

If an earthquake's slip distribution was perfectly known, then calculating a static stress-drop value would be straightforward because strain is proportional to stress. Measuring surface displacements is possible for large, shallow earthquakes in the right tectonic environment, but even then, seismologists cannot directly observe slip distributions at depth. Slip inversion methods have been developed (e.g., Hayes, 2017) to provide some insight into rupture at depth, but these methods are generally applicable only to large, well-instrumented earthquakes. Instead, the most common approaches for estimating stress drop measure dynamic rupture parameters that are proxies for stress drop using seismograms. Although the specific steps vary among studies, most studies follow similar approaches.

First, seismologists select seismograms in which the earthquake is well recorded. Next, they window the seismic phases of interest (e.g., P, S, or coda waves) and determine how to deconvolve the earthquake source signal from station and path effects. Numerous source signal extraction approaches exist depending on data availability and subsurface knowledge. Some approaches just account for attenuation (e.g., Abercrombie, 1995), but others use synthetic green functions to model attenuation and earth structure (e.g., Vallée and Douet, 2016). Other approaches, such

Cite this article as Neely, J. S., S. Park, and A. Baltay (2024). The Impact of Source Time Function Complexity on Stress-Drop Estimates, Bull. Seismol. Soc. Am. XX, 1-13, doi: 10.1785/0120240022

© Seismological Society of America

^{1.} Department of the Geophysical Sciences, The University of Chicago, Chicago, Illinois, U.S.A., (b) https://orcid.org/0000-0003-4029-2979 (JSN); (b) https://orcid.org/ 0000-0002-6660-0047 (SP); 2. United States Geological Survey, Earthquake Science Center, Mountain View, California, U.S.A., https://orcid.org/0000-0002-6514-852X (AB)

^{*}Corresponding author: jneely@uchicago.edu

as the spectral ratio method (e.g., Mueller, 1985), which uses signals from colocated smaller earthquakes as empirical Green's functions, or spectral decomposition (e.g., Andrews, 1986; Shearer *et al.*, 2006), which solves directly for path and site effects using a large number of earthquakes in a region, require no a priori earth structure knowledge.

With the earthquake's source signal extracted (also known as its source time function [STF] or moment-rate function), the seismologist must decide which dynamic rupture value to measure, how to measure it, and which theoretical model to apply to transform the measured value into a stress-drop estimate. Most studies (see Abercrombie, 2021) measure an earthquake's corner frequency (which is theoretically inversely proportional to an earthquake's rupture duration) from its spectral amplitude in the frequency domain. Different spectral amplitude models exist (e.g., Brune, 1970; Boatwright, 1980), and different theoretical relationships between corner frequency and stress drop (e.g., Brune, 1970; Sato and Hirasawa, 1973; Madariaga, 1976) have been proposed. Although these approaches assume different simple, theoretical rupture models, they share a key assumption: an earthquake's corner frequency (and conversely rupture duration) provides insight into its rupture dimensions, which, when combined with its seismic moment, can be used to estimate stress drop. These methods reduce an earthquake's stress drop to a single value (assumed to be the average stress drop on the fault) even though real earthquakes likely have heterogeneous stress release (e.g., Bouchon, 1997).

Each step in the stress-drop estimation procedure introduces uncertainty into the final estimate. The discrepancies between the studies suggest that stress-drop uncertainty might be quite large and poorly accounted for in final estimates. These uncertainties have led to questions about the reliability of the stress-drop parameter (Atkinson and Beresnev, 1997). Although seismologists are aware of the apparent discrepancies between studies (e.g., Abercrombie, 2021), only recently have studies such as the Ridgecrest Community Stress-Drop Validation Study (Baltay *et al.*, 2024) begun systematically exploring the sources and extent of these uncertainties.

These large observed uncertainties may be why seismologists have yet to resolve whether stress drop depends on earthquake magnitude despite numerous studies (for a detailed discussion, see Abercrombie, 2021). Some studies find that average stress drops are constant (with significant scatter) across a range of magnitudes (e.g., Allmann and Shearer, 2009; Cocco et al., 2016), but others have observed systematic changes with magnitude (e.g., Mayeda and Walter, 1996; Malagnini et al., 2014). Neely et al. (2020) noted that two independent studies of the same earthquakes could produce different magnitude trends. Whether earthquake stress drops are self-similar across a range of magnitudes has important implications for our understanding of earthquake processes and hazards. If small and large earthquakes behave the same, then we can simply scale up our observations from small earthquakes to model larger ones.

However, if they are systematically different, then we must rethink how useful our observations from small earthquakes are when modeling large ones, yet the implied physical differences between them would be intriguing.

In this study, we focus on one specific, but previously unquantified, explanation for why stress-drop estimates often differ: earthquake rupture complexity. A study by Neely et al. (2020) showed that independent stress-drop estimates using time-domain and frequency-domain methods produced conflicting results. We apply these two methods to estimate stress drops for nearly 4000 teleseismically recorded earthquakes in the Seismic source ChAracteristics Retrieved from DEConvolving teleseismic body waves (SCARDEC) STF database (Vallée and Douet, 2016; Vallée et al., 2011). We quantify the complexity of the STFs and examine how STF complexity impacts the theoretical relationships between rupture duration and corner frequency and the resulting stress-drop estimates.

STRESS-DROP ESTIMATES FOR SCARDEC EARTHQUAKES

Many studies assume a Brune earthquake source model (Brune, 1970) when estimating stress drop. In the time domain, the Brune model's STF is defined by the duration (T) of its rupture and the seismic moment (M_0) (Fig. 1a),

$$STF(t,t_0,T,M_0) = M_0 \left(\frac{2\pi}{T}\right)^2 (t-t_0) e^{-\frac{2\pi}{T}(t-t_0)} H(t-t_0), \quad (1)$$

in which t is time; t_0 is the onset time of the rupture and $H(t-t_0)$ is the Heaviside function (Liu *et al.*, 2023). In the frequency domain, the spectral amplitude (Ω) of the STF as a function of frequency (f) becomes

$$\Omega(f_{c}, M_{0}) = \frac{M_{0}}{1 + (f/f_{c})^{n}},$$
(2)

in which f_c is the corner frequency and n is the decay rate. For the Brune model, n = 2. Ω is flat at low frequencies with its value corresponding to the seismic moment (M_0) and then decays at a rate of n = 2 for high frequencies (Fig. 1b). The transition from the flat portion to the decaying portion occurs at the corner frequency (f_c) .

Using the formulation from Eshelby (1957), we can calculate earthquake stress drop $(\Delta \sigma)$ in the time domain $(\widehat{\Delta \sigma_T})$ and frequency domain $(\widehat{\Delta \sigma_f})$ as

$$\widehat{\Delta\sigma_T} = \frac{7}{16} \frac{M_0 c^3}{(k\beta T)^3} = \widehat{\Delta\sigma_{f_c}} = \frac{7}{16} \frac{M_0 (f_c)^3}{(k\beta)^3},\tag{3}$$

in which k is a constant depending on the assumed rupture model and c is a constant of inverse proportionality between rupture duration T and corner frequency f_c , and β is the S-wave velocity. The hat symbol indicates that these are estimates of stress drop. Because T and f_c are inversely proportional for

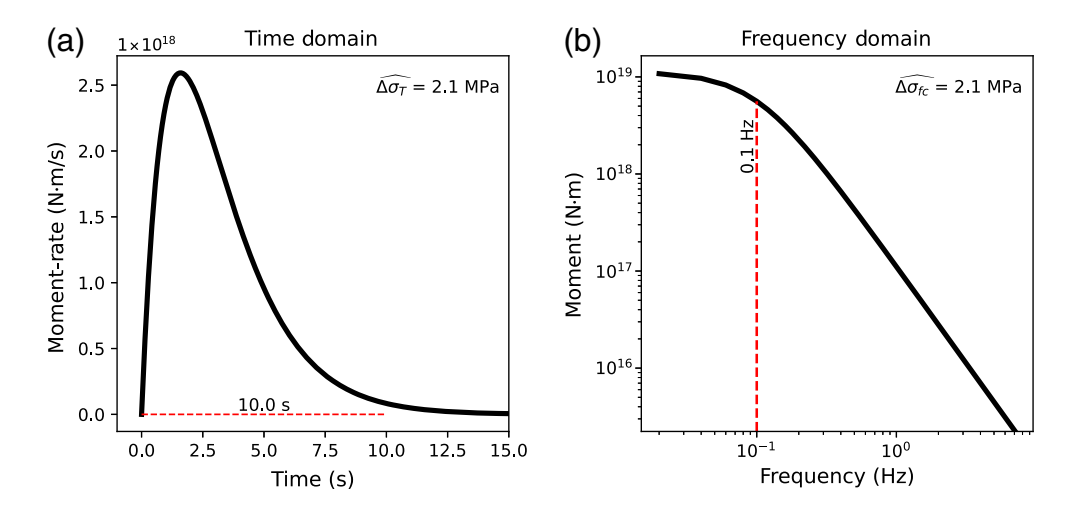


Figure 1. A Brune rupture model example in the time and frequency domains. (a) Brune source in the time domain with rupture duration (T) and resulting stress drop indicated in the top right corner. (b) Same Brune source in the frequency domain (amplitude spectrum) with resulting corner frequency (f_c) and estimated stress drop indicated. Stress-drop calculation here assumes that $T = 1/f_c$. The color version of this figure is available only in the electronic edition.

simple ruptures, the two stress-drop estimates are theoretically equivalent (e.g., Fig. 1) for a simple Brune rupture model. We assume k equals 0.37 (Brune, 1970) and use a fixed β value of 3600 m/s. In practice, to estimate these stress drops, one measures the duration of the STF at some threshold of moment rate in the time domain. In the frequency domain, one would typically fit the Brune (1970) model (equation 2) in log–log space to find the best-fitting M_0 , f_c , and n, though often n is fixed at 2.

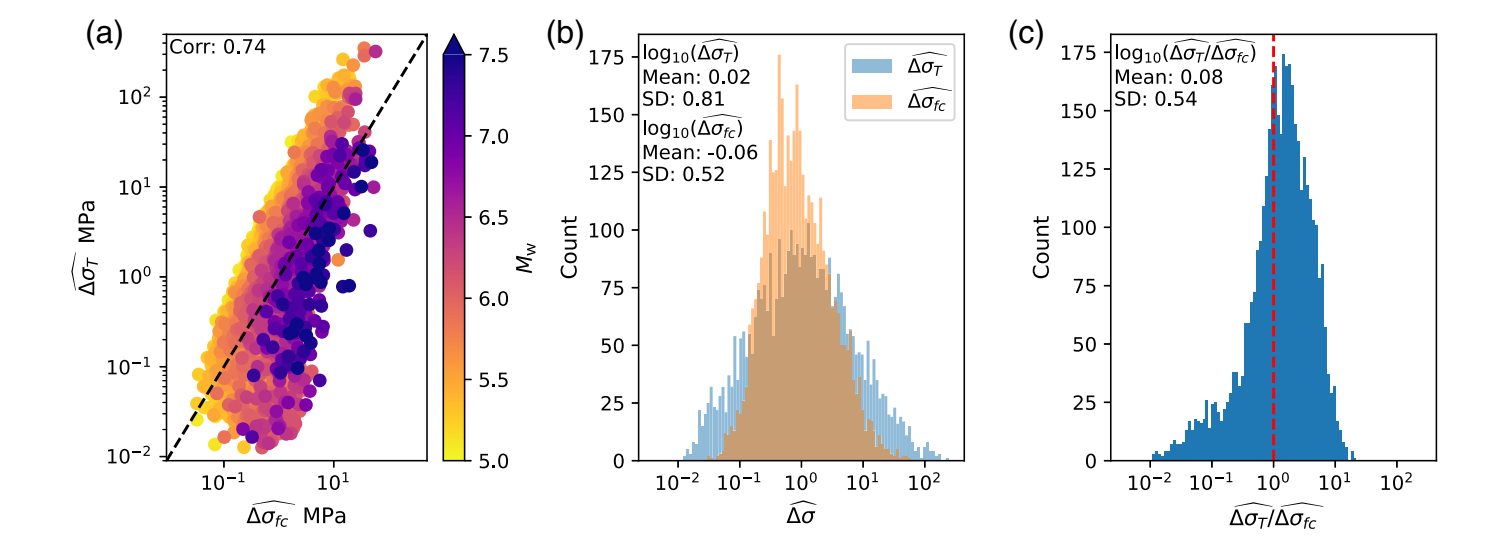
Here, we aim to test the similarities and differences between these two fitting methods. To do so, we consider SCARDEC (Vallée and Douet, 2016) STFs. This database contains 3951 earthquakes ranging from moment magnitude 4.9 to 8.4 and covering the time period from 1992 to 2021. The SCARDEC deconvolution approach uses teleseismically observed body waves to extract earthquake source parameters (Vallée and Douet, 2016). SCARDEC publishes two versions of STF for each earthquake: average and optimal. We use the optimal STF, which is the individual station STF that most closely matches the average of the individual STFs at each station. Although the optimal STF may be influenced by directivity effects, the average STF is depleted at high frequencies, which makes it less ideal for spectral analyses (Vallée and Douet, 2016). Previous studies (e.g. Meier et al., 2021) have noted some limitations with this dataset, such as uncertain earthquake start times and different waveform filtering procedures for earthquakes below and above $M_{\rm w}$ 7. However, in this study, we are primarily concerned with how rupture complexity impacts the time- and frequency-domain estimates, so inconsistencies in processing are less germane to our analysis (but are very important to any interpretations of tectonic trends).

To determine an STF's rupture duration (T), we follow the approach of Courboulex *et al.* (2016), which assumes the

duration is the time between the first and last point of the STF that exceeds 10% of the peak moment rate. We pad the STF with zeros to five times its length to have better constraints on the long-period moment level and then perform a fast Fourier transform to obtain the amplitude spectrum. We resample the spectrum every $0.025 \log_{10}$ units of frequency to distribute more evenly the number of data points above and below the corner frequency. The Nyquist frequency is ~7 Hz for SCARDEC STFs (based on the published STF sampling rates) and is significantly larger than our largest estimated corner frequencies

(~1 Hz). We fit the Brune spectral model (equation 2) with n=2 to solve for the corner frequency f_c . The lower end of the frequency band over which we perform this fitting depends on the time-series length after padding with zeros, but the upper limit is always ~7 Hz. A small earthquake with a padded time series of 50 s would have a minimum frequency of 0.02 Hz. A larger earthquake with a padded time series of 150 s would have a minimum frequency of 0.006 Hz. We fix the seismic moment to the long-period amplitude of the spectra, which we assume is well resolved. With T and f_c , we estimate two different stress drops for each earthquake. We set the constant of inverse proportionality c=0.77 (equation 3) empirically to ensure that the measured rupture duration using the 10% threshold criteria corresponds to the estimated corner frequency for a Brune source (i.e., $c \times T^{-1} = f_c$).

The time-domain $(\Delta \sigma_T)$ and frequency-domain estimates $(\Delta \sigma_f)$ are in general agreement about which earthquakes have higher or lower stress drops (Fig. 2a) based on the correlation of 0.74. If the two estimates were equal, the points would fall on the dashed one-to-one line, but we do observe some scatter. For a given time-domain estimate, larger-magnitude earthquakes appear to be biased toward higher-frequency-domain estimates. A closer look at the distribution of the stress-drop estimates (Fig. 2b) shows the $\Delta \sigma_T$ values are slightly larger on average than $\widehat{\Delta \sigma_f}$ estimates with more variability between events. In \log_{10} units, the average $\Delta \sigma_T$ value is 0.02 (1 MPa), and the average $\Delta \sigma_f$ is -0.06 (0.9 MPa). These averages are in line with other studies when considering the different constants that studies assume (see Cotton et al., 2013). We also observe differences in the standard deviations—0.81 and 0.52 in log₁₀ units for the time- and frequency-domain methods, respectively. The larger standard deviation for the



time-domain method implies a greater variation in stress drop between earthquakes (also known as more scatter). These standard deviations are similar to previously observed differences between earthquakes (Cotton et al., 2013), although the variability for the time-domain estimates is on the high side. The ratio of the two estimates (Fig. 2c) shows just how much the estimates can vary. On average, the estimates do not differ by much, but for individual earthquakes, the time-domain estimate can be almost 10 times larger or up to 100 times smaller than the frequency-domain estimate. Such deviations suggest that there can be considerable uncertainties in the two estimates. The left skew of the distribution may reflect the long tails that are present in some STFs, which increase the measured time duration and decrease the corresponding timedomain stress-drop estimate relative to the frequency-domain estimate.

QUANTIFYING EARTHQUAKE COMPLEXITY

The discrepancies between these two stress-drop estimates may reflect the simplifying assumptions of the Brune source model. In reality, earthquake ruptures can be much more complex, releasing seismic moment in myriad ways. There are numerous ways to quantify the complexity of STFs. Previous studies of SCARDEC STF complexity focused on the number of observable pulses of seismic moment release (Danré *et al.*, 2019; Liu *et al.*, 2023). Others focused on the overall shape of the STF in the time domain using dynamic time warping to cluster the various earthquakes (Yin *et al.*, 2021).

In this study, we define earthquake complexity as the deviation from the simple Brune source model. To measure the complexity in the time domain, we propose a new measure called the Brune relative energy (BRE), which compares the radiated energy of the observed STF with the reference Brune model (in equation 1). The BRE is defined as the ratio of the STF's radiated energy relative to a Brune source pulse with the same seismic moment and rupture duration T,

Figure 2. Stress-drop estimates for SCARDEC earthquakes. (a) Scatter plot of frequency-domain $(\widehat{\Delta\sigma_{f_c}})$ versus time-domain $(\widehat{\Delta\sigma_{T}})$ stress-drop estimates colored by magnitude. The black dashed line is one-to-one line, along which we would naively expect the cloud point to lie. The correlation coefficient is indicated. (b) Histograms of frequency-domain $(\widehat{\Delta\sigma_{f_c}})$ rorange) and time-domain $(\widehat{\Delta\sigma_{T_c}})$ blue) stress-drop estimates. Mean and standard deviation (SD) of the \log_{10} values indicated. (c) Histogram of the ratio of time-domain stress-drop estimates $(\widehat{\Delta\sigma_{T}})$ to frequency-domain $(\widehat{\Delta\sigma_{f_c}})$ estimates for the same earthquake. Mean and standard deviation (SDs) of the \log_{10} values are indicated. The red vertical dashed line indicates 1:1 ratio in which the two stress-drop estimates are identical. The color version of this figure is available only in the electronic edition.

$$BRE = \frac{\int_0^{Sdur} (\ddot{M}_{STF})^2 dt}{\int_0^{Sdur} (\ddot{M}_{Brune})^2 dt}.$$
 (4)

In equation 4, $\dot{M}_{\rm STF}$ is the derivative of the earthquake's STF from SCARDEC and $\ddot{M}_{\rm Brune}$ is the derivative of the ideal Brune STF with the same seismic moment and duration. These are both squared and integrated over the duration of the earthquake STF signal. Therefore, BRE essentially compares the energy of the STF with respect to that of the Brune STF, without any corrections for missing energy at higher, unobserved frequencies. We note that the derivative of the STFs are integrated over the entire earthquake signal (Sdur), which is longer than the duration T defined earlier using the 10% cutoff. This ensures that the small variations in signal complexity at the end of the STF below the 10% threshold are included.

The BRE measure is similar to the radiated energy enhancement factor (REEF) proposed by Ye et al. (2018), except that BRE is normalized relative to the Brune model and not a parabolic source like REEF. A parabolic source radiates the minimum amount of energy for a given duration and seismic moment, and normalizing against a parabolic STF would produce values ~2 to 2.5 times larger. In addition, unlike the REEF, the BRE score makes no adjustment for missing

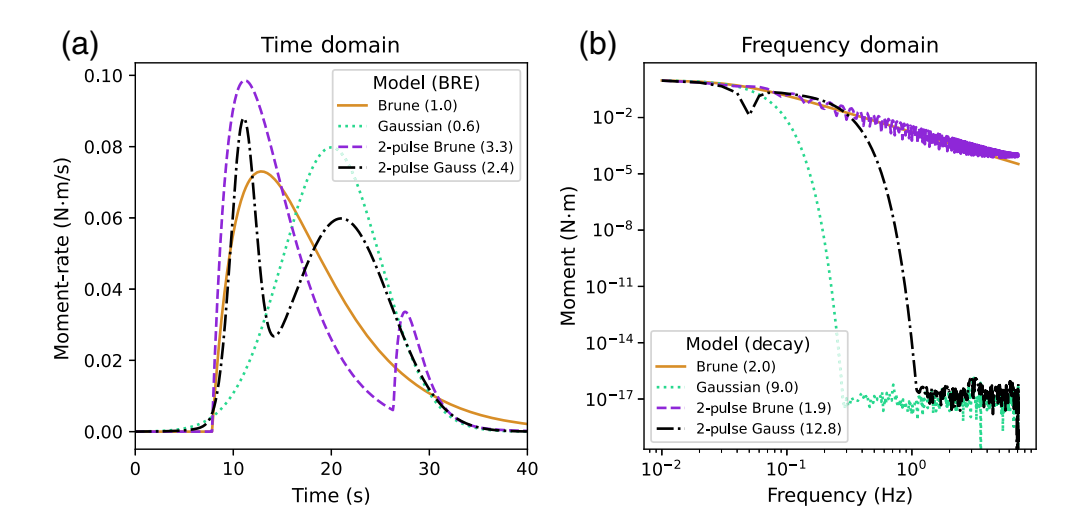


Figure 3. Schematic examples of source time function (STF) complexity. (a) Example of four STFs (Brune, Gaussian, two-pulse Brune, and two-pulse Gaussian STFs) in the time domain with the same duration. Corresponding Brune relative energy (BRE) values indicated in parentheses. All four have the same duration and moment. (b) Corresponding STFs' amplitude spectra with decay values indicated in parentheses. The color version of this figure is available only in the electronic edition.

high-frequency energy, so BRE and REEF are not perfectly comparable. A BRE value of 1 means the STF released the same amount of energy or has the same STF roughness as the Brune model with the same moment and duration. Values <1 indicate that the STF released less energy or is smoother, whereas values >1 indicate it released more energy or is rougher than the Brune STF. Visually, an STF with a BRE <1 looks more like a Gaussian than a Brune STF for the same total moment (Fig. 3a). These symmetric, Gaussian-like ruptures do not release energy as suddenly as a Brune model. Conversely, a BRE >1 can be achieved by distinct pulses of moment release such as two staggered Brune or two staggered Gaussian pulses.

Rupture complexity in the time domain also produces complexity in the frequency domain and deviations from the theoretical Brune amplitude spectrum (Fig. 3b). Such deviations have been quantified previously (e.g., Uchide and Imanishi, 2016), but these analyses have tended to focus on the goodness of fit (i.e., residual values) and not necessarily the overall shape of the spectrum. Such metrics can be influenced by oscillations in the spectrum. For example, even relatively simple ruptures consisting of two Brune pulses produce significant spectral oscillations that are a function of rupture duration and pulse onset timing (Liu et al. 2023), which can result in large residual values compared with those for much more complex ruptures. Thus, we instead propose the spectral decay (n) to characterize the fall-off of the spectrum. We determine this parameter by finding both the f_c and n that best fit the spectral model in equation (2), in which decay is the best-fitting n value. Here again, we are defining the earthquake's complexity relative to its deviation from the simple Brune model in which n = 2.

A decay value of 2 indicates that the spectrum has a shape corresponding to the theoretical Brune model (Fig. 3b). A Gaussian pulse will have a decay value >2 (indicating a relative depletion of energy at high frequencies compared to the Brune model with the same corner frequency). It is worth mentioning that a Gaussian pulse in the time domain, in theory, is also a Gaussian pulse in the frequency domain. However, the discrete numerical sampling of a Gaussian pulse in the time domain leads to an amplitude spectrum that appropriate at low looks frequencies but levels off at high frequencies (green dotted line in Fig. 3b). Fitting a single cor-

ner fall-off spectral model produces a decay value that averages the two slopes, and still results in a value >2. A two-pulse Gaussian model also has a decay much >2 (even though it has a BRE value >1 in the time domain) and an apparent corner that is much higher than the single Gaussian pulse even though they have the same measured duration in the time domain. A two-pulse Brune model, on the other hand, can produce decay values <2. In this case, the Brune model would underestimate the spectra's high-frequency energy. Considering that alternatives to the Brune spectral model like the sharper-cornered Boatwright (1980) model or a double corner-frequency model (e.g., Atkinson, 1993; Ji and Archuleta, 2021) have been proposed, variations from the overall Brune shape are expected.

The BRE and decay metrics go beyond measuring simply the number of pulses or the residual in the spectrum by providing directional information about the deviation from the ideal Brune model. For instance, all four earthquakes in Figure 4 look complex with at least two (or more) clear pulses of moment release. In the time domain, the earthquakes in Figure 4a,e have BRE values that are <1 (i.e., enervated), and the earthquakes in Figure 4c,g have BRE values >1 (i.e., energetic). Upon visual inspection in the time domain, one might classify the earthquakes in Figure 4a,e as less complex than the ones in Figure 4c,g, but in the frequency domain, the earthquakes are more difficult to distinguish. However, they do all have decay values that deviate from the assumed n = 2 model in different directions. These deviations from the Brune model can produce discrepancies in the time- and frequency-domain stress-drop estimates as seen with the first earthquake (Fig. 4a,b), but not always, for the second earthquake's time- and frequencydomain stress-drop estimates (Fig. 4c,d) are similar.

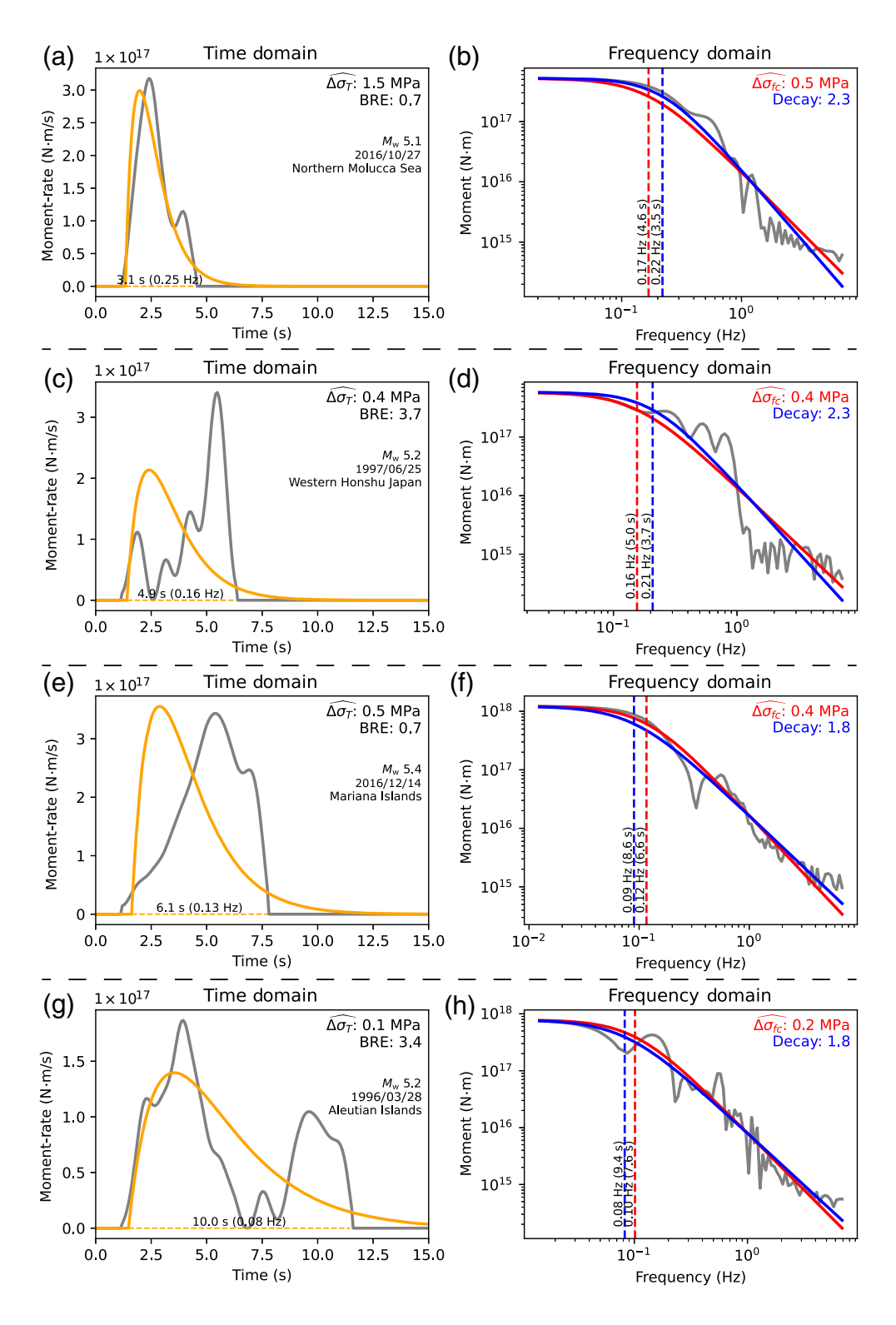


Figure 4. Complexity measures in the time and frequency domains. (a) The real STF for the 2016 $M_{\rm w}$ 5.1 Northern Molucca Sea earthquake (gray) with a rupture duration (T) of ~3.1 s and Brune STF (orange) with the same rupture duration and seismic moment. Estimated time-domain stress drop $(\widehat{\Delta\sigma_T})$ and BRE indicated. Corresponding corner frequency for the measured rupture duration (assuming $f_c=0.77/T$) listed in parenthesis. (b) Amplitude spectrum (gray) for the real STF from panel (a). Corner frequency for the best-fitting Brune model (red solid) is 0.17 Hz, indicated with red dashed line, and the estimated frequency-domain stress drop $(\widehat{\Delta\sigma_{f_c}})$ is indicated at the top right corner. The blue line indicates the best-fitting spectral model ($f_c=0.22$ Hz), in which n is not fixed as 2 (n=2.3). The resulting n and the corner frequency for this model are indicated as decay at the top right corner and the blue dashed line, respectively. The corresponding proportional rupture durations for each corner frequencies are listed in the parentheses. (c–h) The STFs in the time- and frequency-domain metrics for three other earthquakes, which were chosen to display a variety of end-member source behavior. The color version of this figure is available only in the electronic edition.

We have also explored other STF complexity measures (relative to the Brune model) in both the time and frequency domains, including dynamic time warping, cross correlation, Fréchet distance, and mean square error. However, because these complexity measures are unidirectional (values can only increase), they are less informative than the bidirectional (values can increase or decrease) BRE and decay metrics in which both the difference and relative direction can be informative. Furthermore, we have found that these measures do not correlate as well with the stressdrop estimates as do BRE and decay as discussed in the following sections.

INFLUENCE OF STF COMPLEXITY ON STRESS-DROP ESTIMATES

We estimate these two complexity metrics, BRE and decay, for the earthquakes in the SCARDEC database. The typical SCARDEC earthquake does not differ much from the simple Brune model with median BRE and decay values (and 95% confidence intervals from 1000 bootstrapped samples) of 0.97 (0.93 to 1.01) and 1.94 (1.93 to 1.95), respectively. If all earthquakes were truly Brune sources, then the BRE and decay would be 1.0 and 2.0, respectively. These metrics vary substantially for individual earthquakes, and such variations may influence stress-drop estimates. STF BRE values range from 0.3 to 152 and are roughly inversely correlated with the time-domain estimate of stress drop (Fig. 5a). As BRE increases, the time-domain stress-drop estimates decrease, but there is significant scatter.

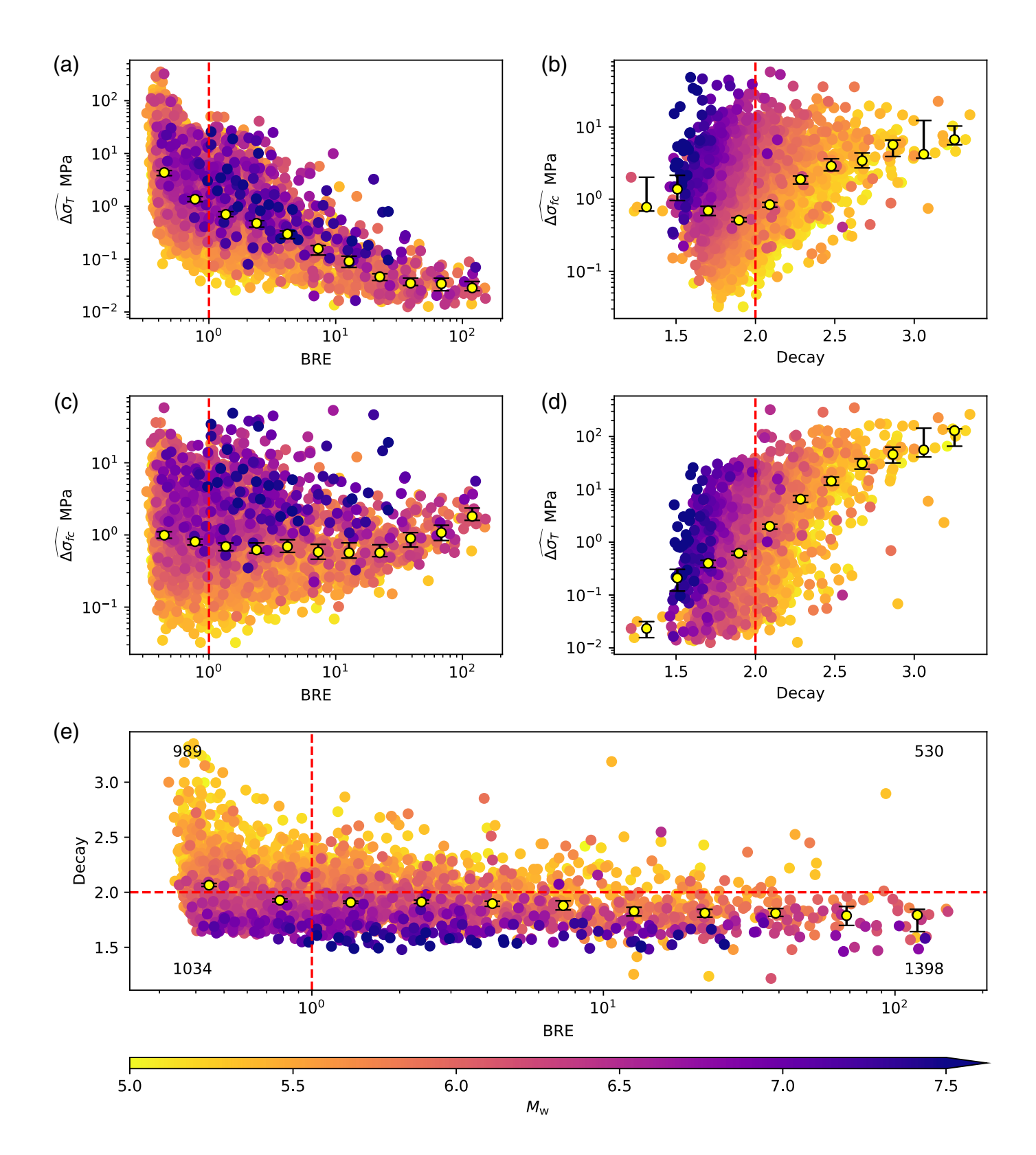


Figure 5. Relationships among the STF complexity metrics and stress-drop estimates. (a) BRE versus time-domain estimates of stress drop $(\widehat{\Delta\sigma_T})$ for SCARDEC STFs. (b) Decay versus frequency-domain estimate of stress drop $(\widehat{\Delta\sigma_{f_c}})$ for SCARDEC STFs. (c) BRE versus frequency-domain estimates of stress drop. (d) Decay versus time-domain estimates of stress drop. (e) BRE versus decay for SCARDEC STFs. In all panels, the red dashed vertical and

horizontal lines indicate a BRE of 1 and a decay of 2, respectively, which corresponds to a Brune model (decay of 2 and same radiated energy). The number of earthquakes in each quadrant is indicated. All points are colored by earthquake magnitude. Median values indicated by yellow circles with 95% bootstrapped confidence intervals. The color version of this figure is available only in the electronic edition.

Decay and frequency-domain stress-drop estimates (Fig. 5b) show a more complicated relationship. Decay estimates span from 1.2 to 3.4. For decay values <~2, the median frequency-domain stress-drop estimate decreases with an increasing decay. But for decay values >~2, the median frequency-domain stress-drop estimate increases with an increasing decay. We also observe a magnitude-dependent trend, with larger-magnitude earthquakes (> $M_{\rm w}$ 6.0) having decay values near or <2. Note that a handful of the earthquakes have decay values <1.5, the theoretical minimum limit for finite radiated energy proposed by Walter and Brune (1993). We have kept these earthquakes in our analysis because this decay value only represents the slope of the spectra below the Nyquist frequency (~7 Hz), and they may have a steeper decay (assuming a multicorner model) at higher frequencies as $f \rightarrow \infty$.

Although we observe a relationship between BRE and the time-domain stress-drop estimates, we do not observe a similar relationship for the frequency-domain stress-drop estimates and BRE (Fig. 5c). Frequency-domain stress-drop estimates are relatively flat with an increasing BRE values. However, there is a trend of increasing time-domain estimates with an increasing decay (Fig. 5d), albeit with significant scatter.

When we plot BRE and decay against each other for all the earthquakes, we find that there is not a clear correlation between the two complexity measures (Fig. 5e). Such an absence of correlation indicates that our two complexity metrics measured in the time and frequency domains capture independent information about the STF complexity. A plurality of earthquakes (1398) fall in the lower-right quadrant (decay <2 and BRE >1), indicating that they tend to be more energetic than a Brune model with a shallower spectral decay shape. Nearly half of the earthquakes fall in either the upper-right (decay >2 and BRE >1) or lower-left (decay <2 and BRE <1) quadrants. At first glance, a decay >2 and a BRE >1 (or conversely a decay <2 and a BRE <1) would appear incongruous because of the radiated energy implications. However, an earthquake with decay >2 can still be more energetic than a Brune model over the observed frequency band if the earthquake's corner frequency (without the decay = 2 assumption) is larger than the Brune model's corner frequency (see Fig. 4d). Conversely, an earthquake with a decay <2 and a BRE <1 (such as the earthquake in Fig. 4e,f) is possible depending on the specific shape of the STF.

DISCREPANCIES BETWEEN THE TIME- AND FREQUENCY-DOMAIN METHOD ESTIMATES CORRESPOND TO STF COMPLEXITY

As shown in Figure 2, the two stress-drop estimation methods can result in different values. We find that a significant part of the scatter in Figure 2a and the discrepancies shown in Figure 2b, c can be explained by the STF complexity metrics we propose in this study. In other words, the relative values of these two different stress-drop estimates vary systematically based on the complexity metrics (Fig. 6). When BRE <1, the time-domain

stress-drop estimates are larger than the corresponding frequency-domain estimates (Fig. 6a). Conversely, when BRE >1, the frequency-domain estimates are larger. When BRE = 1, the two estimates are nearly identical because the STF is quite similar to a Brune model. The tight clustering of points in Figure 6b shows that BRE is a good predictor of the relative values of the two different stress-drop estimation methods. Yoshida and Kanamori (2023, in their fig. 12C) found similar results for the REEF complexity metric in their analysis of 1736 $M_{\rm w}$ 3–7 earthquakes in Japan.

Although not quite as clear, decay also provides insights into the relative values of the two stress-drop estimates. Larger decay values produce relatively larger time-domain estimates, and smaller decay values produce relatively larger frequency-domain estimates (Fig. 6c). An increase in the decay value increases the ratio of the two estimates initially but starts to level off for the decay values >2.5 (Fig. 6d). Earthquake magnitude does not appear to influence these complexity-stress-drop relationships.

HOW DOES STRESS DROP CHANGE WITH EARTHQUAKE MAGNITUDE?

Our analyses show that magnitude-stress-drop trends depend on the methodology (Fig. 7). Using a binned median (sampled every 0.25 magnitude unit bins with 95% confidence intervals obtained via 1000 bootstrap samples), we observe a slight increase with magnitude for the time-domain stress-drop estimates from 2.1 MPa for the smallest earthquakes to 5.3 MPa for $M_{\rm w}$ 7.0 (Fig. 7a) before decreasing again for larger earthquakes. This slight trend is not very pronounced and therefore does not necessarily disagree with a previous analysis on a subset of the SCARDEC database by Vallée (2013), who found that stress drop was magnitude independent. BRE shows a steady increase with earthquake magnitude, although there are large uncertainties in the median BRE above $M_{\rm w}$ 7.0 (Fig. 7b). In contrast, frequency-domain stress-drop estimates (Fig. 7c) show a clear increase in stress drop with magnitude, from \sim 0.5 MPa at $M_{\rm w}$ 5.25 to 4.4 MPa at $M_{\rm w}$ 7.0. At the same time, we find that the median decay value systematically decreases with magnitude (Fig. 7d). Small earthquakes (less than $M_{\rm w}$ 5.5) have a median decay greater than 2 and larger earthquakes (above $M_{\rm w}$ 5.5) have a median decay <2. These systematic complexity variations with magnitude may reflect the frequency filtering that SCARDEC applies based on magnitude. Different high-pass filter and signal truncation criteria are applied in the SCARDEC analysis depending upon whether the earthquake is greater or less than $M_{\rm w}$ 7.

For the SCARDEC STFs, the observed magnitude dependence of the frequency-domain stress-drop estimates (Fig. 7c) is likely not real and simply reflects the systematic changes in the shape of the spectral amplitudes (Fig. 7d). The stress drops in Figure 7c are based on an estimated corner frequency assuming a fixed decay of n = 2. Van Houtte and Denolle (2018) noted

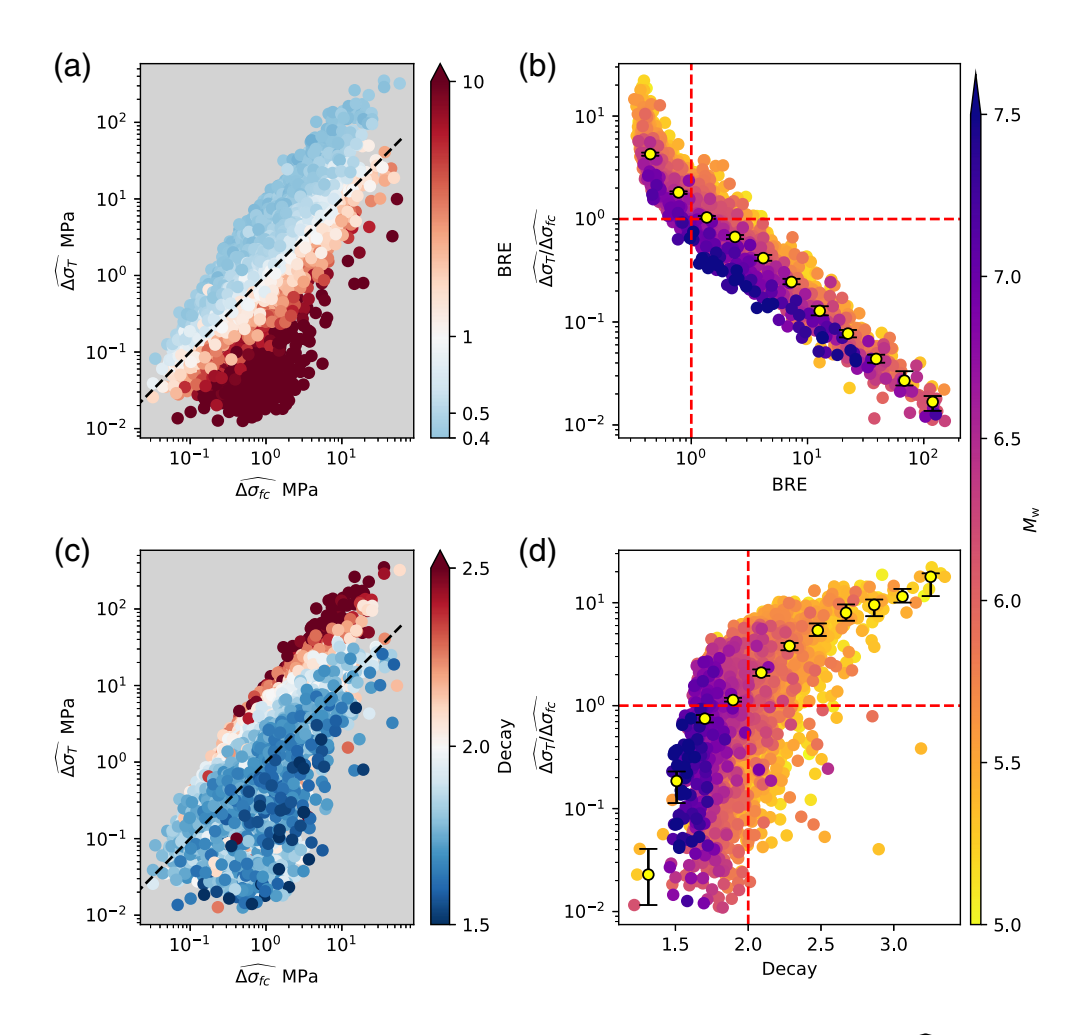


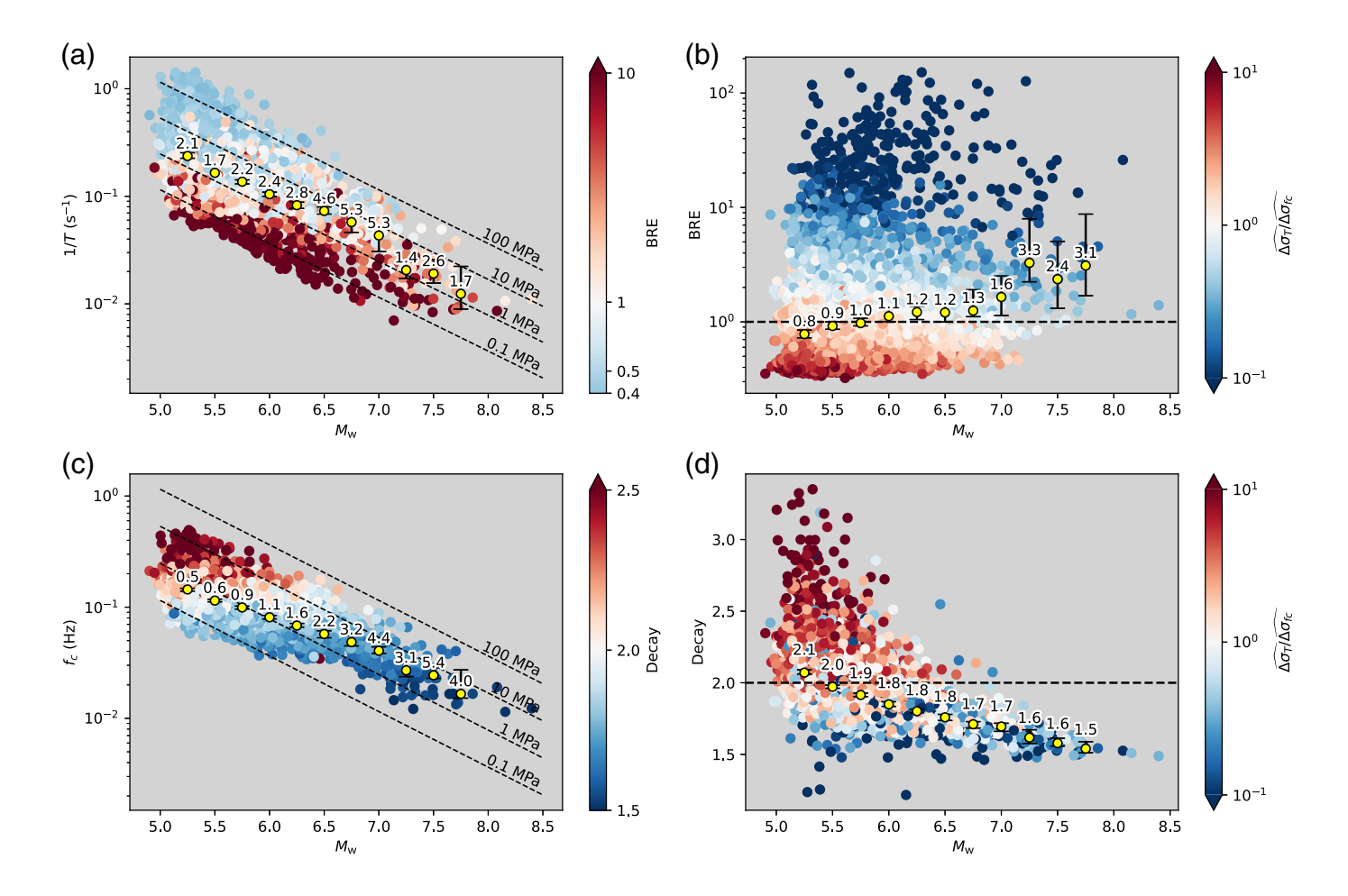
Figure 6. Relative stress-drop estimates versus complexity. (a) Scatter plot of frequency-domain $(\widehat{\Delta\sigma_f}_c)$ and time-domain $(\widehat{\Delta\sigma_f})$ stress-drop estimates. The black dashed line is one-to-one line. The color indicates BRE value. (b) Scatter plot of BRE versus ratio of time- and frequency-domain stress-drop estimates. The red vertical dashed line corresponds to theoretical Brune STF (BRE = 1), and horizontal dashed line indicates when the two stress-drop estimates are in agreement. The color indicates earthquake magnitude. (c) Same as panel (a) except that the colors indicate decay value. (d) Same as panel (b) except that the stress-drop ratio is plotted against decay and red vertical dashed line indicates the decay value (n = 2) for Brune STFs. The color version of this figure is available only in the electronic edition.

that assuming a fixed decay of n = 2 could bias the corner frequency estimate. If we allow the decay to vary freely when estimating corner frequency, we find that the magnitudedependent trend in the stress-drop estimates becomes greatly muted (Fig. 8a). These revised stress-drop estimates now range from 0.6 MPa at $M_{\rm w}$ 5.25 to 1.1 MPa at $M_{\rm w}$ 7.0. However, caution should be applied when interpreting these stress-drop estimates because it is not clear how corner frequencies relate to stress drop when spectral decays vary between the earthquakes. Figure 8b shows why the stress drop may appear to vary with magnitude when fitting a Brune model (with n = 2) to spectra with systematically decreasing decays with magnitude. Figure 8b contains four idealized spectra with a decreasing decay with magnitude from n = 2.2 for an M_w 5.0 to n = 1.7 for an M_w 6.5 (similar to what we observe with the SCARDEC data). We have set the true corner frequencies to scale with the negative cube of the seismic moment, which corresponds to a constant stress-drop value. However, when we fit a Brune model (with decay fixed to n=2), the estimated corner frequencies now scale as -4.7 of the seismic moment. This change in slope of the estimated corner frequencies produces a systematic magnitude dependence with stress drop increasing with magnitude.

We also observe that for a fixed magnitude, the estimated corner frequency increases with a spectral decay (Fig. 8a). In Figure 8c, we show how this systematic trend explains the U-shaped frequency-domain stress-drop patterns observed in Figure 5b. We present three spectra with the same moment but with corner frequencies that increase with the spectral decay. The spectrum with the smallest decay n = 1.5 has the smallest corner frequency, the n = 2.0spectrum is next, and the n = 2.5 spectrum has the largest corner frequency. We then fit a Brune model (with a decay fixed at n = 2) to the spectra and estimate the corner frequencies. The Brune model overestimates the corner fre-

quency of the n=1.5 spectrum and underestimates the corner frequency of the n=2.5 spectrum. Although the true corner frequencies increase with the decay, the order of the estimated corner frequencies is now switched. The estimated corner frequency of the n=1.5 spectrum is now larger than the n=2 spectrum, therefore producing a larger stress-drop estimate. This relative reordering of the estimated corner frequencies for different decay values likely explains the observed median frequency-domain stress-drop trends (Fig. 5b) in which spectra with the decay near 2 have lower estimated stress drops than decays above and below 2. Note that the corner frequency's proximity to the Nyquist frequency will determine how much the n=2 assumption over- or underestimates the true corner frequency.

Our results provide important new insights into the assumptions of earthquake self-similarity. In the time domain, the BRE



complexity (Fig. 7b) does seem to vary systematically with the magnitude. These median BRE differences are not large enough to produce any strong stress-drop magnitude trends (Fig. 7a). In the frequency domain, assuming a fixed decay with n = 2 suggests that the earthquake stress drops are not self-similar (Fig. 7c). This finding is similar to some past frequency-domain studies, which have also found an increase in stress drop with a magnitude (see references in Abercrombie, 2021). However, Trugman and Shearer (2017) and Trugman (2020) observed that although a fixed decay of n = 2 can produce this magnitude-dependent trend, with a smaller, fixed constant decay $(n \sim 1.8)$, the earthquake stress drops are self-similar. By accounting for the variable decays (Fig. 8a), we show that the stress drop (via the corner frequencies) is (nearly) self-similar, but the decay is not (Fig. 7d). This suggests that only some aspects of the earthquake rupture (corner frequency) are selfsimilar, but others (spectral decay) are not. One should therefore exercise caution when interpreting stress-drop results in the presence of varying earthquake complexity.

REAL VERSUS APPARENT SOURCE COMPLEXITY

Whether the earthquake complexities assessed in this study are real or artifacts, however, remains unresolved and seems to depend on how STF complexity is quantified. Here, we have shown that different measures of complexity (BRE and decay)

Figure 7. Stress drop and complexity as a function of magnitude. (a) Earthquake magnitude versus the inverse of rupture duration (1/T) colored by BRE. The dashed lines indicate lines of constant stress drop. The yellow circles indicate median value (for 0.25 magnitude unit bins) with 95% confidence intervals calculated from 1000 bootstrapped samples. (b) Magnitude versus BRE colored by ratio of time-domain and frequency-domain stress-drop estimates. As in panel (a), the median and the two standard errors are indicated. The dashed line (BRE = 1) corresponds to the theoretical Brune model. (c) Same as panel (a) except that the vertical axis is corner frequency (f_c) and the color indicates decay. (d) Same as panel (b) except that the vertical axis is decay, and the dashed line (decay = 2) corresponds to Brune models. The color version of this figure is available only in the electronic edition.

in different domains (time and frequency) produce magnitude-complexity trends. In a previous time-domain study of the SCARDEC database, Danré et al. (2019) found that the number of distinguishable subevents increased with magnitude, and our observation of a slightly increasing BRE with magnitude may reflect a similar trend. However, frequency-domain residual analyses (Uchide and Imanishi, 2016) have shown that when sufficiently resolved, small earthquakes can be complex and deviate from an assumed Brune source model. Yoshida and Kanamori (2023) examined a wide magnitude range of earthquakes in Japan and observed no systematic changes in complexity with a magnitude based on the REEF complexity

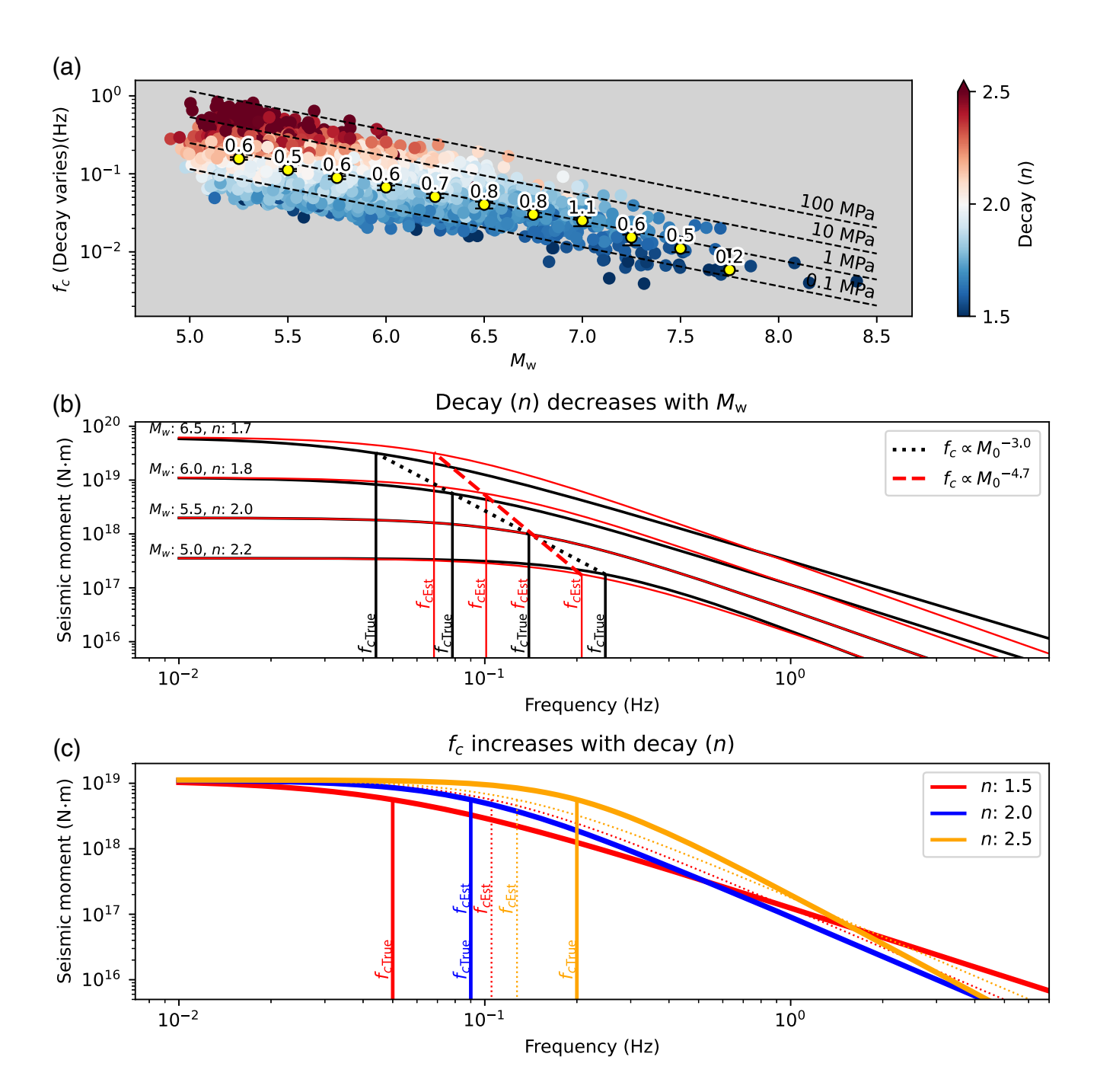


Figure 8. Impacts of variable decay on estimating corner frequencies. (a) Estimated corner frequencies (with variable decays) versus earth-quake magnitude. Color indicates decay value. Lines of constant stress drop are indicated. Median values (yellow circles) with bootstrapped 95% confidence intervals. Corresponding median stress-drop value is indicated. (b) Impact of variable decay on estimating corner frequency assuming a fixed decay (n=2) model. The solid black lines indicate theoretical spectra with decay decreasing with increasing magnitude. The black dashed line indicates that the true corner frequencies (f_{cTrue}) scale with the negative cube of seismic moment. The red lines are best-fitting Brune spectra (n=2) for the black curves. The estimated corner

frequencies are indicated in red (f_{cEst}) and scale with the negative 4.7 of seismic moment, producing an apparent increase in stress drop with magnitude. (c) Demonstration of how the variable decays (n) impact stress-drop estimates for a fixed seismic moment. The solid thick lines indicate theoretical spectra with corner frequencies (f_{cTrue}) that increase with decay. The dashed spectra indicate the best fitting Brune model (n=2) with the vertical dashed lines indicating the estimated corner frequencies (f_{cEst}). Note that the order of f_{cEst} differs from f_{cTrue} . The color version of this figure is available only in the electronic edition.

parameter, which normalizes the radiated energy by a parabolic (rather than Brune) source model. Pennington *et al.* (2023) observed that both time- and frequency-domain complexity increase with a magnitude for small microearthquakes ($M_{\rm w}$ <3). However, they attributed this apparent magnitude trend to resolution issues for the smallest earthquakes, which may make them appear simpler than they actually are.

It is possible that the observed decay (and BRE) changes with magnitude are in fact real. Smaller magnitude earthquakes may have relatively large decay values. However, the relatively low sampling rate of the STFs (~14 Hz) and the use of teleseismic data, which lack high-frequency information, may not be able to resolve the complexities in smaller earthquakes—similar to what Pennington *et al.* (2023) proposed. This could explain the larger decay rates for the smaller earthquakes because the higher frequencies are depleted. These magnitude patterns may also arise from the different processing approaches SCARDEC applies depending on the earthquake's magnitude (Vallée and Douet, 2016). Regardless of the origin of the complexities, however, we emphasize that the complexities' contributions to the variations and trends in stress-drop estimates remain unchanged.

CONCLUSIONS

Our analyses have shown that the assumption that time- and frequency-domain stress-drop estimates are equivalent fails when applied to complex, real earthquakes. Stress-drop estimates for the same earthquake can vary by more than an order of magnitude. We examine two bidirectional complexity measurements—BRE in the time domain and decay in the frequency domain—with systematic relationships between the two stressdrop estimates and implications for magnitude scale-invariance trends. Larger BRE values clearly correspond to smaller timedomain stress-drop estimates compared with frequency-domain estimates. BRE slightly varies with magnitude, and decay systematically decreases with increasing magnitude. Failure to account for this systematic variation in spectral shape creates apparent (but false) increases in frequency-domain stress-drop estimates with magnitude. Whether this decay-magnitude trend reflects real variations or limitations of the SCARDEC data analyzed remains unresolved.

DATA AND RESOURCES

All data used in this study are available via the SCARDEC source time function website (http://scardec.projects.sismo.ipgp.fr, last accessed December 2022).

DECLARATION OF COMPETING INTERESTS

The authors declare no competing interests.

ACKNOWLEDGMENTS

The authors thank Rachel Abercrombie for her insightful feedback. The authors also thank two anonymous reviewers for their comments. This material is based on work supported by the National Science Foundation under Award Number 2204102. Any use of trade, firm, or product names is for descriptive purposes only and does not imply endorsement by the U.S. Government.

REFERENCES

- Abercrombie, R. E. (1995). Earthquake source scaling relationships from -1 to 5 $M_{\rm L}$ using seismograms recorded at 2.5-km depth, *J. Geophys. Res.* **100**, 24,015–24,036, doi: 10.1029/95JB02397.
- Abercrombie, R. E. (2021). Resolution and uncertainties in estimates of earthquakes stress drop and energy release, *Phil. Trans. Roy. Soc. Lond. A* **379**, doi: 10.1098/rsta.2020.0131.
- Allmann, B. P., and P. M. Shearer (2009). Global variations of stress drop for moderate to large earthquakes, *J. Geophys. Res.* **114**, no. B13, doi: 10.1029/2008JB005821.
- Andrews, D. J. (1986). Objective determination of source parameters and similarity of earthquakes of different size, in *Earthquake Source Mechanics*, Vol. 37, 259–267, doi: 10.1029/GM037p0259.
- Atkinson, G. M. (1993). Earthquake source spectra in eastern North America, *Bull. Seismol. Soc. Am.* **83**, 1778–1798.
- Atkinson, G. M., and I. Beresnev (1997). Don't call it stress drop, Seismol. Res. Lett. 68, 3-4, doi: 10.1785/gssrl.68.1.3.
- Baltay, A., R. Abercrombie, S. Chu, and T. Taira (2024). The SCEC/USGS community stress drop validation study using the 2019 Ridgecrest earthquake sequence, *Seismica* 3, no. 1, doi: 10.26443/seismica.v3i1.1009.
- Boatwright, J. (1980). A spectral theory for circular seismic sources: Simple estimates of source dimension, dynamic stress drop, and radiated seismic energy, *Bull. Seismol. Soc. Am.* **70**, 1–28.
- Boore, D. M. (1983). Stochastic simulation of high-frequency ground motions based on seismological models of the radiated spectra, *Bull. Seismol. Soc. Am.* **73**, 1865–1894.
- Bouchon, M. (1997). The state of stress on some faults of the San Andreas system as inferred from near-field strong motion data, *J. Geophys. Res.* **102**, no. B6, 11,731–11,744, doi: 10.1029/97JB00623.
- Brune, J. N. (1970). Tectonic stress and the spectra of seismic shear waves from earthquakes, *J. Geophys. Res.* **75**, 4997–5009, doi: 10.1029/JB075i026p04997.
- Causse, M., L. A. Dalguer, and P. M. Mai (2014). Variability of dynamic source parameters inferred from kinematica models of past earthquakes, *Geophys. J. Int.* **196**, no. 3, 1754–1769, doi: 10.1093/gji/ggt478.
- Cocco, M., E. Tinti, and A. Cirella (2016). On the scale dependence of earthquake stress drop, *J. Seismol.* **20,** 1151–1170, doi: 10.1007/s10950-016-9594-4.
- Cotton, F., R. Archuleta, and M. Causse (2013). What is sigma of the stress drop? *Seismol. Res. Lett.* **84**, 42–48, doi: 10.1785/0220120087.
- Courboulex, F., M. Vallée, M. Causse, and A. Chounet (2016). Stress-drop variability of shallow earthquakes extracted from a global database of source time functions, *Seismol. Res. Lett.* 87, 912–918, doi: 10.1785/0220150283.
- Danré, P., J. Yin, B. P. Lipovsky, and M. A. Denolle (2019). Earthquakes within earthquakes: Patterns in rupture complexity, *Geophys. Res. Lett.* **46**, doi: 10.1029/2019GL083093.
- Eshelby, J. D. (1957). The determination of the elastic field of an ellipsoid, and related problems, *Proc. Math. Phys. Sci.* **241**, 376–396, doi: 10.1098/rspa.1957.0133.

- Hayes, G. P. (2017). The finite, kinematic rupture properties of great-sized earthquakes since 1990, *Earth Planet. Sci. Lett.* **468**, 94–100, doi: 10.1016/j.epsl.2017.04.003.
- Ji, C., and R. J. Archuleta (2021). Two empirical double-corner-frequency source spectra and their physical implications, *Bull. Seismol. Soc. Am.* 111, no. 2, 737–761, doi: 10.1785/0120200238.
- Kanamori, H., and D. L. Anderson (1975). Theoretical basis of some empirical relations in seismology, *Bull. Seismol. Soc. Am.* 65, 1073–1095.
- Kemna, K. B., A. Verdecchia, and R. M. Harrington (2021). Spatio-temporal evolution of earthquake static stress drop values in the 2016–2017 central Italy seismic sequence, *J. Geophys. Res.* 126, no. 11, e2021JB022566, doi: 10.1029/2021JB022566.
- Liu, M., Y. Huang, and J. Ritsema (2023). Characterizing multisubevent earthquakes using the Brune source model, *Bull. Seismol. Soc. Am.* **113**, no. 2, 577–591, doi: 10.1785/0120220192.
- Madariaga, R. (1976). Dynamics of an expanding circular fault, *Bull. Seismol. Soc. Am.* **66**, 639–666, doi: 10.1785/BSSA0660030639.
- Malagnini, L., K. Mayeda, S. Nielsen, S.-H. Yoo, I. Munafo, C. Rawles, and E. Boschi (2014). Scaling transition in earthquake sources: A possible link between seismic and laboratory measurements, *Pure Appl. Geophys.* 171, 2685–2707, doi: 10.1007/s00024-013-0749-8.
- Mayeda, K., and W. Walter (1996). Moment, energy, stress drop, and source spectra of western United States earthquakes from regional coda envelopes, *J. Geophys. Res.* **101,** 11,195–11,208, doi: 10.1029/96JB00112.
- Meier, M. A., J. P. Ampuero, E. Cochran, and M. Page (2021). Apparent earthquake rupture predictability, *Geophys. J. Int.* **225**, no. 1, 657–663, doi: 10.1093/gji/ggaa610.
- Mueller, C. S. (1985). Source pulse enhancement by deconvolution of an empirical Green's function, *Geophys. Res. Lett.* **12**, no. 1, 33–36, doi: 10.1029/GL012i001p00033.
- Neely, J. S., S. Stein, and B. D. Spencer (2020). Large uncertainties in earthquake stress-drop estimates and their tectonic consequences, *Seismol. Res. Lett.* **91**, no. 4, 2320–2329, doi: 10.1785/0220200004.
- Pennington, C. N., Q. Wu, X. Chen, and R. E. Abercrombie (2023). Quantifying rupture characteristics of microearthquakes in the Parkfield area using a high-resolution borehole network, *Geophys. J. Int.* **233**, 1772–1785, doi: 10.1093/gji/ggad023.
- Sato, T., and T. Hirasawa (1973). Body wave spectra from propagating shear cracks, *J. Phys. Earth* **21,** no. 4, 415–431, doi: 10.4294/jpe1952.21.415.

- Shearer, P. M., G. A. Prieto, and E. Hauksson (2006). Comprehensive analysis of earthquake source spectra in southern California, *J. Geophys. Res.* **111,** no. B6, doi: 10.1029/2005jb003979.
- Trugman, D. T. (2020). Stress-drop and source scaling of the 2019 Ridgecrest, California, earthquake sequence, *Bull. Seismol. Soc. Am.* **110**, no. 4, 1859–1871, doi: 10.1785/0120200009.
- Trugman, D. T., and P. M. Shearer (2017). Application of an improved spectral decomposition method to examine earthquake source scaling in southern California, *J. Geophys. Res.* 122, no. 4, 2890–2910, doi: 10.1002/2017JB013971.
- Uchide, T., and K. Imanishi (2016). Small earthquakes deviate from the omega-square model as revealed by multiple spectral ratio analysis, *Bull. Seismol. Soc. Am.* **106**, no. 3, 1357–1363, doi: 10.1785/0120150322.
- Vallée, M. (2013). Source time function properties indicate a strain drop independent of earthquake depth and magnitude, *Nat. Commun.* **4,** 2606, doi: 10.1038/ncomms3606.
- Vallée, M., and D. Douet (2016). A new database of source time functions (STFs) extracted from the SCARDEC method, *Phys. Earth Planet. In.* **257**, 149–157, doi: 10.1016/j.pepi.2016.05.012.
- Vallée, M., J. Charléty, A. M. G. Ferreira, B. Delouis, and J. Vergoz (2011). SCARDEC: A new technique for the rapid determination of seismic moment magnitude, focal mechanism and source time functions for large earthquakes using body-wave deconvolution, *Geophys. J. Int.* 184, 338–358, doi: 10.1111/j.1365-246X.2010.04836.x.
- Van Houtte, C., and M. Denolle (2018). Improved model fitting for the empirical Green's function approach using hierarchical models, *J. Geophys. Res.* **123**, no. 4, 2923–2942, doi: 10.1002/2017JB014943.
- Walter, W. R., and J. N. Brune (1993). Spectra of seismic radiation from a tensile crack, *J. Geophys. Res.* **98**, no. B3, 4449–4459, doi: 10.1029/92JB02414.
- Ye, L., H. Kanamori, and T. Lay (2018). Global variations of large megathrust earthquake rupture characteristics, *Sci. Adv.* **4**, doi: 10.1126/sciadv.aao4915.
- Yin, J., Z. Li, and M. A. Denolle (2021). Source time function clustering reveals patterns in earthquake dynamics, *Seismol. Res. Lett.* 92, no. 4, 2343–2353, doi: 10.1785/0220200403.
- Yoshida, K., and H. Kanamori (2023). Time-domain source parameter estimation of $M_{\rm w}$ 3–7 earthquakes in Japan from a large database of moment-rate functions, *Geophys. J. Int.* **234**, 243–262, doi: 10.1093/gji/ggad068.

Manuscript received 5 February 2024 Published online 21 August 2024